Modeling and Incorporation of System Response Functions in 3D Whole Body PET

Adam M. Alessio, *Member IEEE*, Paul E. Kinahan, *Senior Member IEEE*,
and Thomas K. Lewellen, *Senior Member IEEE*
University of Washington Medical Center, Seattle, WA

***Abstract*-- Appropriate application of spatially variant system models can correct for degraded resolution response and mispositioning errors. This work explores the detector blurring component of the system model for a whole body PET system and extends this factor into a more general system response function to account for other system non-idealities such as the influence of FORE rebinning. We model the system response function as a 3 dimensional function that blurs in the radial and axial dimension and is spatially variant in radial location. This function is derived from Monte Carlo simulations and incorporates inter-crystal scatter, crystal penetration, and the blurring due to FORE rebinning. The improved system model is applied in a modified OSEM algorithm to reconstruct FORE rebinned, fully 3D PET data into images with improved resolution and quantitative accuracy.**

I. Introduction

Spatially variant system models have been shown to be advantageous in image reconstruction algorithms for high-resolution small animal PET systems [1-4]. Appropriate incorporation of these system models can correct for degraded, variant resolution response and mispositioning errors (particularly at the edge of the FOV). This work explores the detector blurring component of the system model for a whole body (human) PET system and extends this factor into a more general system response function (SRF) to account for other system non-idealities such as the influence of FORE rebinning.

In an effort to improve reconstructions from FORE rebinned PET data, we model the SRF as a 3 dimensional function that blurs in the radial and axial dimension and is spatially variant in radial location. We measure the SRF from Monte Carlo simulations and apply the new system model in a modified OSEM algorithm to reconstruct images with improved resolution and reduced quantitative errors.

II. Description of the System Response Function

The detector blurring factor has also been described as the coincident aperture function [3], detector response function [5], or system kernel [1]. These different functions incorporate varying system effects including inter-crystal scatter, crystal penetration, photon pair non-colinearity, depth dependent sensitivity, and non-uniform sinogram sampling. We propose a more general blurring factor denoted as the system response function (SRF). In a fully determined system model, this function is unique for each detector pair and to each volume location that contributes to the pair. In fully 3D PET, this equates to a 7 dimensional function with 4 dimensions to describe the line integral domain and 3 dimensions to describe the imaging volume domain. One choice of variables appears in figure 1 to describe SRF $S(u, v, \phi, \theta; x, y, z)$ where (u, v) defines the point on one detector surface where the coincident bin with azimuthal and axial angle (ϕ, θ) intersects. And, (x,y,z) defines the location in the volume that contributes to this coincident bin.

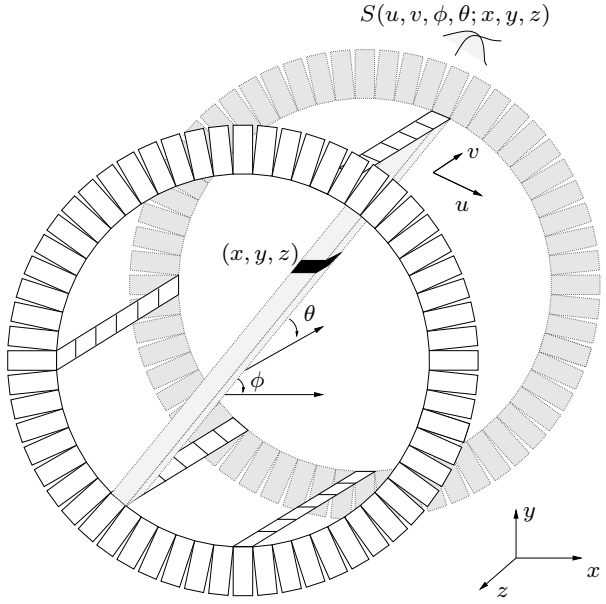

Fig 1. Illustration of fully characterized system response function, S, where (u, v) defines the point on one detector surface where the coincident bin with azimuthal and axial angle (ϕ, θ) intersects. And, (x,y,z) defines the location in the volume that contributes to this coincident bin.

Most algorithms use spatially invariant system models resulting in sub-optimal reconstructions. These simple models could be considered as one dimensional system response

Department of Radiology, University of Washington, Seattle, WA 98195 USA (telephone: 206-598-4521 email: aalessio@u.washington.edu)
This work supported by NIH grants CA74135 and CA42593

functions. Past efforts to model a spatially variant system blurring factor often use the 2 dimensional function, $SRF_{2Dsimple}(s;s_v)$, which blurs along radial bins in the sinograms (s, the distance between the z axis and the projection of the line onto a transaxial plane) and is spatially variant in radial distance s_v. The subscript v denotes the variables that parameterize the originating volume location as opposed to the line integrals.

This work presents a 3 dimensional function $SRF_{3Dimproved}(s,z;s_v)$ which blurs along radial bins (s) and axial planes (z) and is variant along radial bins (s_v). This function incorporates the system effects of inter-crystal scatter, crystal penetration and the blurring due to FORE rebinning.

III. Acquiring the System Response Function

The system response function can be determined through analytical derivations [3, 6, 7], with Monte Carlo simulations [2, 8, 9], or empirically [1, 4, 5]. In theory, the empirical approach of physically measuring the system response to a collimated point source leads to the most accurate description of the system. We employed a Monte Carlo simulation method [10] with the intention that it could be translated into a feasible empirical setup to accurately define the system model for a real scanner.

Using SimSET modified to account for discrete detector elements, we simulated a whole body PET scanner with a geometry and detection system similar to the GE Advance. We positioned single point sources at different radial and axial locations in the imaging FOV and collected fully 3D emission data. The point sources were not collimated, making this a feasible approach for real data measurements. Each fully 3D data set was FORE rebinned into 2D PET data, $y(s,\phi,z)$, to lead to a fast, practical reconstruction method. As expected, analysis of the rebinned sinograms showed that the system blurs the coincident lines in the three dimensions of the rebinned data. Moreover, the radial positioning of the source followed by the axial positioning cause the greatest variations in the system response. Consequently, we choose to use a kernel that only blurs in radial and axial bins to model the system. Figure 2 presents the $SRF_{3Dimproved}$ at different radial positions.

The following abbreviated summary outlines the steps performed to approximate the 3 dimensional $SRF_{3Dimproved}(s,z;s_v)$. Four fully 3D data sets were simulated from a point source at 4 different radial positions and FORE rebinned into sets of direct and cross planes. For a fixed ϕ, the (s, z) view of this data is the projection view of the data, as opposed to a sinogram view, and provides the desired system response information. The 4 data sets lead to measured response functions (s, z) at 4 radial positions s_v. The response functions at the remaining s_v are approximated by parameterizing the simulated (s, z) functions with discrete cosine transform coefficients. Then, a least-squares fit to a linear relationship amongst the coefficients from the 4 simulated response functions leads to coefficient values at all s_v and consequently, the complete $SRF_{3Dimproved}$.

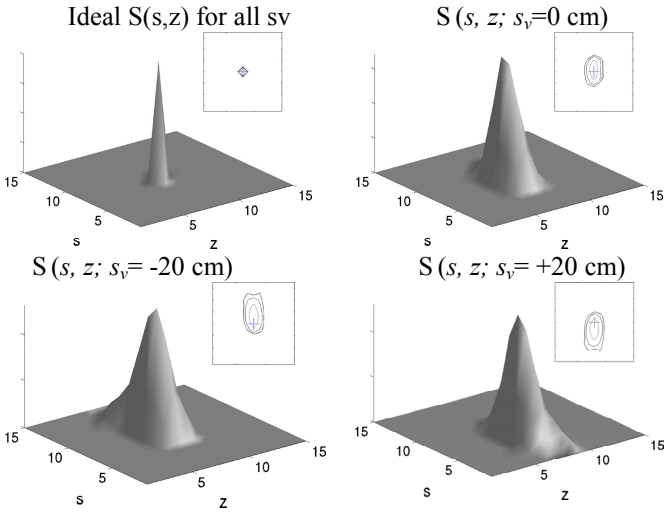

Fig 2. $S_{3D\ improved}(s, z; s_v)$ at several radial locations for a transaxial FOV[-27.5cm, 27.5cm]. The inlaid *(s,z)* contour plots mark the center of the ideal with a cross and show the half, fifth and tenth maximum contours.

IV. Application

The SRF was incorporated into the system matrix in a modified OSEM algorithm. One possible approach would be to use a factorized model and apply this blurring term in the forward and back projector [8], requiring a two dimensional convolution for each call to the system matrix. Since, memory was not a constraint, we precompute the sparse blurred system matrix and store only the non-zero entries. The applied $SRF_{3Dimproved}$ blurring function consisted of a 9×5 kernel that varied at all radial bin positions.

Conventional 2D OSEM performs a complete reconstruction of one transaxial plane then reconstructs the next transaxial plane. With this SRF, the forward projection step requires image estimates from neighboring planes, so the algorithm was modified to perform one iteration on a plane then one iteration on the next plane, effectively updating all transaxial planes during a single iteration.

We test this new method with two separate simulation studies. First, we preformed Monte Carlo simulations of a phantom containing 17 point sources at 3 different radial positions in the FOV. The fully 3D Monte Carlo generated data was FORE rebinned and reconstructed with FBP conventional OSEM, and OSEM with our improved system response function to gauge the resolution improvements with the new method.

Secondly, we preformed analytical simulations of fully 3D data from a whole-body phantom to evaluate the bias vs. noise tradeoffs [11]. These data sets (emission and transmission scans) were blurred with a 4 dimensional function (with slight variations from the 3 dimensional function used in the

reconstruction to account for the possible inaccuracies in the modeling of the system response) to simulate the non-idealities of the detection system. We generated 50 independent realizations from this phantom with typical clinical noise levels. We performed attenuation correction of the 3D data, FORE rebinning, and then reconstructed with 2D FBP, (AW) OSEM [12], or (AW)OSEM with the improved SRF (referred to as OSEM w/ SRF for brevity).

V. Results

A. Monte Carlo Simulations

Figure 3 presents the reconstructions of the point source phantoms with FBP, conventional OSEM, and OSEM w/ $SRF_{3Dimproved}$. The surface plots show the shape of a point source located at s_v = 20cm in the transverse and axial plane.

Figures 4 and 5 present a more systematic analysis of the resolution improvements. Figure 4 shows the average transaxial full width half maximum (FWHM) and full width tenth maximum versus the radial distance from the center of the FOV for the three reconstruction methods. Figure 5 presents a volumetric figure displaying the radius of the sphere inscribed in the half and tenth maximum of the points at varying radial distance. Figures 3-5 show that the new method improves the resolution of the system by as much as 15% over OSEM towards the edge of the FOV.

B. Analytical Simulations

Figure 6 shows the true image and sample reconstructions of simulated data from the whole-body phantom. This phantom contains 24 spherical lesions of 1cm, 2cm, and 3cm diameters and 2 varying contrast levels (3.5:1 and 1.5:1). The lesions were positioned in varying background levels of the lung, thorax and liver region.

Figure 7 displays the average bias in the mean values of the tumor regions of interest versus the tumor size. These points were generated from unsmoothed reconstructions of noise-free data of the whole-body phantom to determine of the potential quantitative improvement with the new method. The plot shows that no improvement can be expected with small lesions, while ~18% improvement in mean bias is possible with larger lesions.

Figure 8 presents curves of the different reconstruction methods with varying smoothing parameters. For FBP, the cutoff frequency of the Hanning window was varied from 100% to 20% in 20% increments. For OSEM and OSEM w/ improved SRF, the post-reconstruction smoothing filter was varied from no smoothing to a 15 mm Gaussian filter in 2.5 mm increments. OSEM was performed with 12 subsets and 7 iterations and OSEM w/ SRF was performed with 12 subsets and 13 iterations. These iteration parameters were chosen because the change in RMSE (between reconstructions and the true image) per iteration stopped changing at this point and both methods yielded images with similar noise properties. It should be noted that the OSEM w/ SRF method requires more iterations to reach this final image.

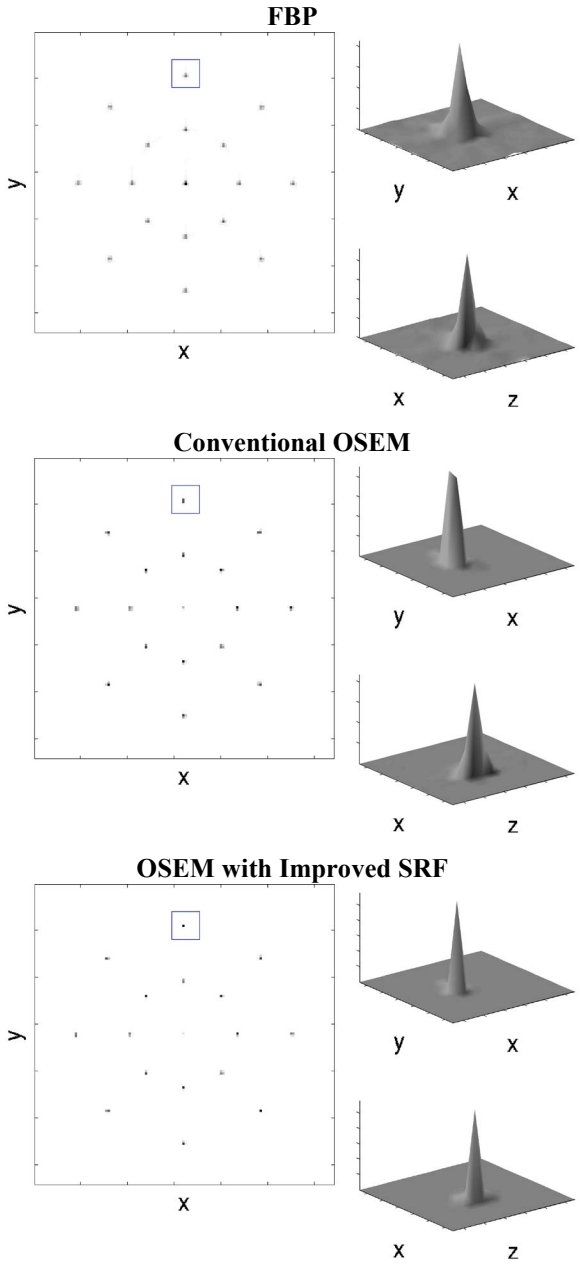

Fig 3. Reconstructions of simple phantom with point sources at 0cm, 10 cm and 20cm from center of FOV. Two surface plots show transaxial and axial slices through a single point. Our proposed method leads to reconstructions with improved resolution.

The top plot in figure 8 shows the average bias in the mean value of each tumor region of interest versus the variance in the mean values. Each datum point is generated from reconstructions of 50 noise realizations and represents the average bias across the 24 lesion sites. The bottom plot in figure 8 shows the average bias in the max value of each tumor region of interest. The max value was evaluated because it is

often used for calculating the standardized uptake values in quantitative studies. The OSEM w/ SRF method results in ~10% gains for some noise levels in terms of mean values and less significant gains in terms of max values.

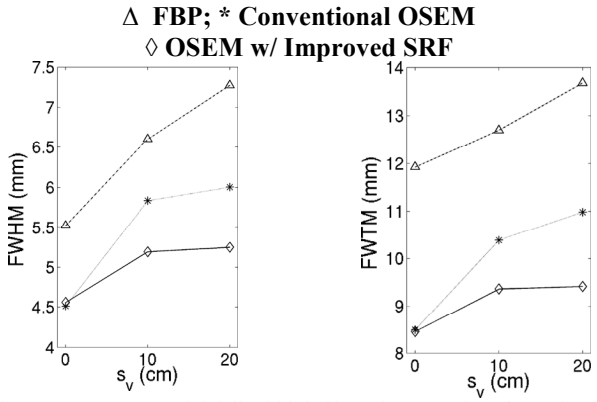

Fig 4. Average transaxial full width half maximum and tenth maximum of the reconstructed point sources. Note that our proposed method yields an ~10% improvement in resolution over conventional OSEM at locations away from center of FOV.

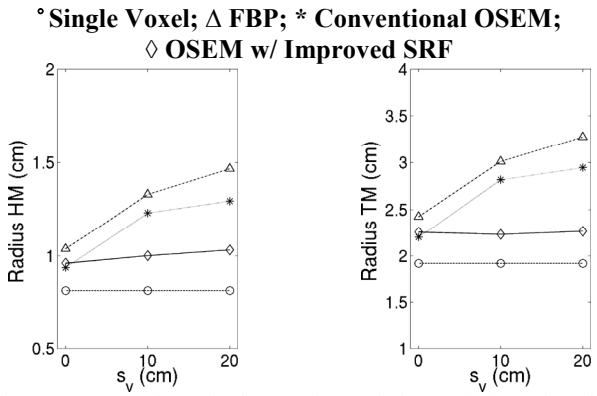

Fig 5. Presents volumetric figures for resolution analysis. Plots the average radius of a sphere inscribed in the half maximum and tenth maximum of each point source. Note the consistent resolution of the OSEM w/ improved SRF method throughout FOV

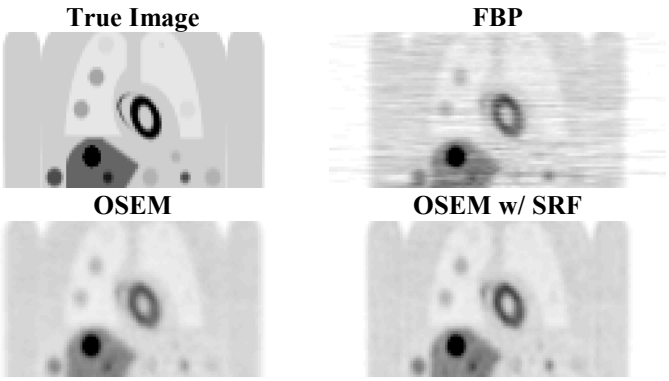

Fig 6. Coronal slice through sample reconstructions from analytically simulated fully 3D data of a phantom containing 24 spherical lesions of 1cm, 2cm, and 3cm diameters and varying contrast levels (3.5:1 and 1.5:1). OSEM reconstructions post smoothed with 10mm Gaussian.

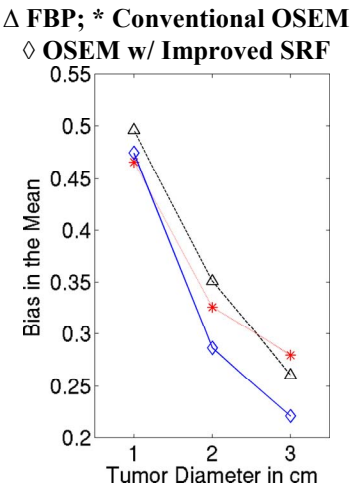

Fig 7. Plot shows biases in the mean values of all the tumors in unsmoothed reconstructions of noise-free data versus tumor size (standard error on these points range from 0.05 to 0.06). The OSEM w/SRF method does not improve the 1cm spherical lesion bias, but does improve the bias of 2cm and 3cm lesions by ~15%.

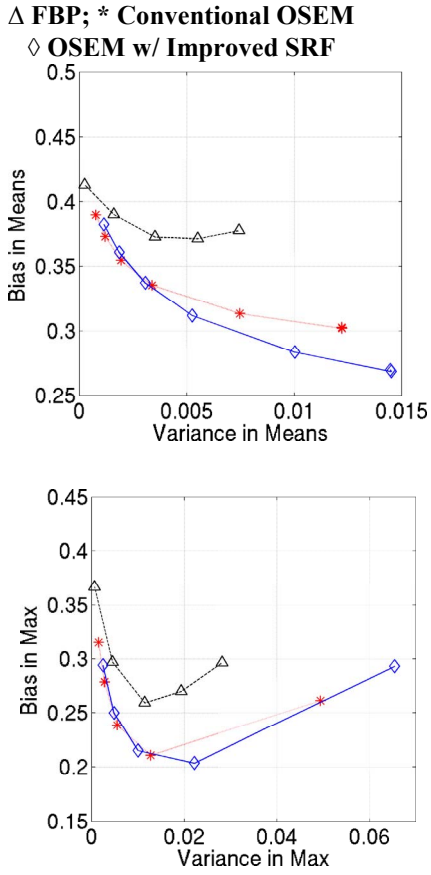

Fig 8. Analysis of quantitative accuracy of the OSEM w/SRF. Each datum point generated from reconstructions of 50 noise realizations. Top plot shows the mean of the bias of the mean values of each tumor region versus the variance in these mean values. Bottom plot shows the mean of bias of the max values of each tumor versus variance of max values. Each curve formed from varying the smoothing parameter of the reconstruction algorithm.

VI. Conclusions

With FWHM and mean tumor value bias gains of approximately 10%, the use of a 3D spatially variant system blurring term with OSEM provides improved reconstructions both in terms of resolution and quantitative accuracy. As expected, the improvements are more significant away from the center of the FOV.

The system response modeling in this work was performed with Monte Carlo simulations. The positive results shown here will motivate our future efforts to model the system response on a real system with a variation of the approach proposed in section II.

The new method requires a less-sparse system matrix causing a computational time increase of approximately seven times per iteration. Consequently, in future work, we intend to analyze simpler system blurring terms, such as a 2D kernel, to determine if we can achieve these marked improvements over conventional OSEM with less computational demands.

VII. References

[1] T. Frese, N. C. Rouze, C. A. Bouman, K. Sauer, and G. D. Hutchins, "Quantitative comparison of FBP, EM, and Bayesian reconstruction algorithms for the IndyPET scanner," *IEEE Trans Med Imaging*, vol. 22, pp. 258-76, 2003.

[2] J. Qi, R. M. Leahy, S. R. Cherry, A. Chatziioannou, and T. H. Farquhar, "High-resolution 3D Bayesian image reconstruction using the microPET small-animal scanner," *Physics in Medicine and Biology*, vol. 43, pp. 1001, 1998.

[3] D. Schmitt, B. Karuta, C. Carrier, and R. Lecomte, "Fast point spread function computation from aperture functions in high-resolution positron emission tomography," *IEEE Trans Med Imaging*, vol. 7, pp. 2-12, March 1988.

[4] K. Lee, P. E. Kinahan, J. A. Fessler, R. S. Miyaoka, and T. K. Lewellen, "Pragmatic Image Reconstruction for the MiCES Fully-3D Mouse Imaging PET Scanner," presented at Presented at: 2003 IEEE Nuclear Science Symposium and Medical Imaging Conference, Portland, OR, 2003.

[5] V. V. Selivanov, Y. Picard, J. Cadorette, S. Rodrigue, and R. Lecomte, "Detector response models for statistical iterative image reconstruction in high resolution PET," *IEEE Trans Nuclear Science*, vol. 47, pp. 1168-1175, June 2000.

[6] D. Strul, R. B. Slates, M. Dahlbom, S. R. Cherry, and P. K. Marsden, "An improved analytical detector response function model for multilayer small-diameter PET scanners," *Phys Med Biol*, vol. 48, pp. 979-994, April 2003.

[7] Z. Liang, "Detector response restoration in image reconstruction of high resolution positron emission tomography," *IEEE Trans Med Imaging*, vol. 13, pp. 314-321, June 1994.

[8] E. U. Mumcuoglu, R. M. Leahy, S. R. Cherry, and E. Hoffman, "Accurate geometric and physical response modelling for statistical image reconstruction in high resolution PET," presented at Proc. of IEEE Nucl. Sci. Symp. and Med. Imaging Conf., 1996.

[9] E. Veklerov, J. Llacer, and E. J. Hoffman, "MLE reconstruction of a brain phantom using a Monte Carlo transition matrix and a statistical stopping rule," *IEEE Trans Nuclear Science*, vol. 35, pp. 603-607, 1998.

[10] T. K. Lewellen, R. L. Harrison, and S. Vannoy, "The SimSET Program in Monte Carlo Calculations," in *Monte Carlo Calculations in Nuclear Medicine*, M. Ljungberg, S. Strand, and M. King, Eds.: IOP Publishing, Philadelphia, PA, 1998, pp. 77-92.

[11] C. Comtat, P. E. Kinahan, M. Defrise, C. Michel, C. Lartizien, and D. W. Townsend, "Simulating whole-body PET scanning with rapid analytical methods," *IEEE Nuclear Science Symposium*, vol. 3, pp. 1260-1264, 1999.

[12] X. Liu, C. Comtat, C. Michel, P. Kinahan, M. Defrise, and D. Townsend, "Comparison of 3-D Reconstruction With 3D-OSEM and with FORE+OSEM for PET," *IEEE Trans Med Imaging*, vol. 20, pp. 804-814, August 2001.